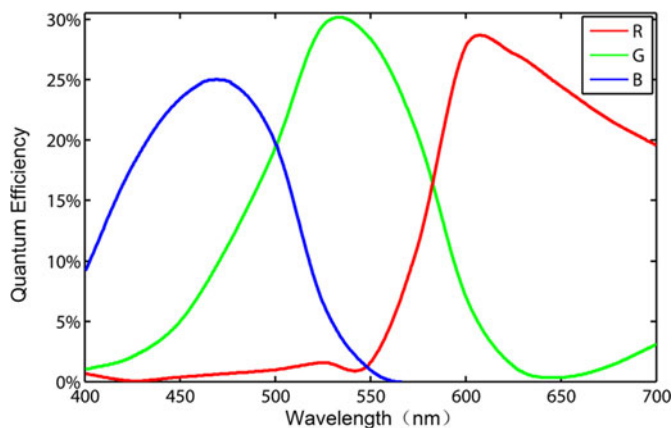


# Multispectral Stokes Imaging Polarimetry Based on Color CCD

Volume 8, Number 5, October 2016

Mingxuan Yu  
Tiegen Liu  
Hesong Huang  
Haofeng Hu  
Bingjing Huang



DOI: 10.1109/JPHOT.2016.2599006

1943-0655 © 2016 IEEE

# Multispectral Stokes Imaging Polarimetry Based on Color CCD

Mingxuan Yu, Tiegeng Liu, Hesong Huang, Haofeng Hu,  
and Bingjing Huang

<sup>1</sup>College of Precision Instrument and Opto-Electronics Engineering, Tianjin University,  
Tianjin 300072, China.

<sup>2</sup>Key Laboratory of Opto-Electronics Information Technical, Tianjin University, Ministry of  
Education, Tianjin 300072, China.

DOI:10.1109/JPHOT.2016.2599006

1943-0655 © 2016 IEEE. Translations and content mining are permitted for academic research only.  
Personal use is also permitted, but republication/redistribution requires IEEE permission.  
See [http://www.ieee.org/publications\\_standards/publications/rights/index.html](http://www.ieee.org/publications_standards/publications/rights/index.html) for more information.

Manuscript received June 17, 2016; accepted August 7, 2016. Date of publication August 12, 2016; date of current version September 8, 2016. This work was supported by the National Natural Science Foundation of China (61405140), the National Instrumentation Program under Grant 2013YQ030915, the Natural Science Foundation of Tianjin (15JCQNJC02000), and the Project sponsored by the Scientific Research Foundation for the Returned Overseas Chinese Scholars. The work of H. Hu was supported by the Fondation Franco-Chinoise pour la Science et ses Applications and the China Scholarship Council. Corresponding author: H. Hu (haofeng\_hu@tju.edu.cn).

**Abstract:** In this paper, we propose a method for multispectral imaging polarimetry based on a color charge-coupled device (CCD), which can simultaneously measure the Stokes vectors at three wavelengths without significantly increasing the complexity of the system and the procedure for the polarimetry. We perform the experiment of imaging polarimetry at three wavelengths and the experiment of target classification based on multispectral imaging polarimetry. The experiment results demonstrate the feasibility of the proposed method, as well as the superiority of this method in target classification and detection.

**Index Terms:** Multispectral polarimetry, Stokes vector, color charge-coupled device (CCD), classification

## 1. Introduction

Imaging polarimetry can obtain the polarization information that is not visible in classical intensity images. Therefore, it has many applications in target detection, remote sensing, and biomedical imaging [1]–[6]. In recent years, multispectral imaging polarimetry [7]–[9], which can measure the polarization information of the scene at different wavelengths, has demonstrated to be an effective optical detection technique. In particular, by combing the polarization information and the spectral information, the performance of target detection can be improved. However, the spectral filter, dispersion element or multiple imaging channels have to be employed in the multispectral imaging polarimetry system [10]–[12], and the procedure of measuring the polarization information has to be repeated for each wavelength [7], [13]. Besides, the multispectral single-shot polarimeter can only acquire the polarimetric information at a single pixel or a linear array of pixels [14], [15], and thus, the procedure of scanning has to be involved to obtain the polarimetric information of a 2-D scene. These factors significantly increase the complexity of the polarimetric system, and, in addition, the procedure of measuring the Stokes vectors for multiple wavelengths becomes much more complex and time consuming, compared with that for single wavelength.

In this paper, based on the characteristic of the color charge-coupled device (CCD) that it can simultaneously measure the light intensities at different wavelengths by RGB channels, we propose the method of multispectral imaging polarimetry based on color CCD, which can simultaneously measure the Stokes vectors at three wavelengths. In this method, we consider the cross-talk effect between RGB channels to make sure the retrieved intensity signals and the measured Stokes vectors are undistorted. We perform the experiment of imaging polarimetry at three wavelengths to verify the feasibility of the proposed method. In addition, we perform the experiment target classification based on multispectral imaging polarimetry, and we compare the performances of target classification at one wavelength and at three wavelengths.

## 2. Stokes Polarimetry at a Single Wavelength

For the passive polarimetry system, the polarization state of the light scattered by the target can be defined as Stokes vector  $\mathbf{S}$ . The scattered light from the target will be analyzed by the polarization state analyzer (PSA), which is a generalized polarizer with the eigenstate of  $\mathbf{T}$ . The light intensity measured by the sensor should be [2]

$$i = \frac{1}{2} \mathbf{T}^T \mathbf{S} \quad (1)$$

where the superscript  $T$  refers to the transpose operator.

Considering the typical Stokes polarimetry [2], [3], four intensity measurements at four different eigenstates of PSA are required to obtain the full Stokes vector, and the four measured light intensities can be expressed as

$$i_m = \frac{1}{2} \mathbf{T}_m^T \mathbf{S}, \quad m \in [1, 4]. \quad (2)$$

The measured light intensities can be also written in a matrix form as

$$\mathbf{I} = \begin{bmatrix} i_1 \\ i_2 \\ i_3 \\ i_4 \end{bmatrix} = \frac{1}{2} \begin{bmatrix} \mathbf{T}_1^T \\ \mathbf{T}_2^T \\ \mathbf{T}_3^T \\ \mathbf{T}_4^T \end{bmatrix} \mathbf{S} = \mathbf{W} \mathbf{S} \quad (3)$$

where  $\mathbf{W}$  is the measurement matrix composed by four different eigenstates  $\mathbf{T}$  of PSA. The polarization state of the scattered light  $\mathbf{S}$  can thus be estimated as [14]

$$\mathbf{S} = \mathbf{W}^{-1} \mathbf{I}. \quad (4)$$

In this way, one can measure the Stokes vector at a certain wavelength.

## 3. Multispectral Stokes polarimetry Based on Color CCD

The Stokes polarimetry for one single wavelength mentioned above can be extended for measuring the Stokes vectors at different wavelengths, taking into account that the eigenstate of PSA  $\mathbf{T}$ , as well as the Stokes vector, could be wavelength dependent.

In this work, we propose a method of multispectral imaging polarimetry based on a color CCD, in which the target is illuminated by the light beam with three different wavelengths corresponding to three color channels (R, G, and B channels) of the color CCD, respectively. In this case, we assume these three wavelengths are  $\lambda_1$ ,  $\lambda_2$  and  $\lambda_3$  respectively, and the Stokes vector of the scattered light at these wavelengths can be expressed as

$$\mathbf{S}_{\lambda_i} = \mathbf{W}_{\lambda_i}^{-1} \mathbf{I}_{\lambda_i}, \quad i \in [1, 3] \quad (5)$$

where  $\mathbf{S}_{\lambda_i}$  and  $\mathbf{I}_{\lambda_i}$  refers to the Stokes vector and the measured intensities at the wavelength of  $\lambda_i$ , respectively, while  $\mathbf{W}_{\lambda_i}$  refers to the measurement matrix at the wavelength of  $\lambda_i$ . It needs to be

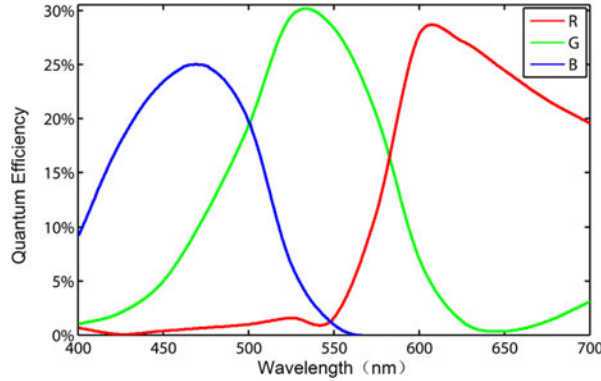


Fig. 1. Quantum efficiencies of RGB channels of the color CCD (AVT Stingray F-33C).

noticed in (5) that the measurement matrix  $W_{\lambda_i}$  could be wavelength depended, due to the possible wavelength dependence of the retarder in PSA.

Besides, due to the cross-talk effect of the quantum efficiency between RGB channels, a color CCD always get the distorted light intensities in practice. Let us take the color CCD of AVT Stingray F-033C for example to illustrate this cross-talk effect. The quantum efficiencies of RGB channels of the CCD at different wavelengths are shown in Fig. 1. It can be seen from Fig. 1 that the quantum efficiencies for RGB channels overlap with each other in some spectral regions. Therefore, the green light with the wavelength of 525 nm, for example, could not only generate the signal in the green (G) channel, and it can generate the considerable signals in the blue (B) and red (R) channels.

In order to compensate the cross-talk effects of the color CCD mentioned above, we introduce a compensation matrix  $K$  to correct the distorted signals measured by the color CCD into a true one. We denote the true light intensities of three wavelengths passing through PSA at the state of  $\mathbf{T}_i$  to be a 3-dimensional vector  $\mathbf{I}_i^{\text{True}}$ , and the three sensor signals in RGB channels measured by the color CCD to be a 3-D vector  $\mathbf{I}_i^{\text{CCD}}$ . The relation between  $\mathbf{I}_i^{\text{True}}$  and  $\mathbf{I}_i^{\text{CCD}}$  can be expressed as

$$\mathbf{I}_i^{\text{CCD}} = K \mathbf{I}_i^{\text{True}}, \quad i \in [1, 4] \quad (6)$$

Based on (6), one can compensate the cross-talk effects to deduce the true light intensities of the three wavelengths. Consequently, the Stokes vectors at three wavelengths can be estimated, respectively, based on (5).

#### 4. Experimental Setup of Multispectral Imaging Polarimetry Based on Color CCD

To achieve the multispectral polarimetry method mentioned above, we design an imaging polarimetry system, which includes three laser sources with three different wavelengths of  $\lambda_1$ ,  $\lambda_2$  and  $\lambda_3$  respectively. The experimental setup is shown in Fig. 2. In our experiment, the three wavelengths are 633 nm, 532 nm, and 450 nm, which correspond to the red, green, and blue channels of the color CCD, respectively. The PSA in our system is composed by a linear polarizer and a rotating wave plate. By changing the orientations of the linear polarizer and the wave plate, the eigenstate of PSA  $\mathbf{T}$  can be adjusted, which will be discussed in detail in the following. The type of the color CCD is AVT Stingray F-033C, whose quantum efficiencies are shown in Fig. 1.

The Muller matrix of a linear polarizer can be expressed as

$$M_P(\theta_P) = \frac{1}{2} \begin{bmatrix} 1 & \cos 2\theta_P & \sin 2\theta_P & 0 \\ \cos 2\theta_P & \cos^2 2\theta_P & \sin 2\theta_P \cos 2\theta_P & 0 \\ \sin 2\theta_P & \sin 2\theta_P \cos 2\theta_P & \sin^2 2\theta_P & 0 \\ 0 & 0 & 0 & 0 \end{bmatrix} \quad (7)$$

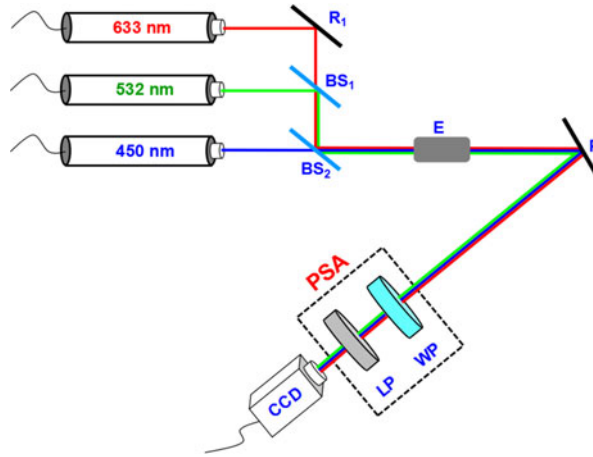


Fig. 2. Experimental setup of Stokes imaging polarimetry system. R: reflectors; BS: beam splitter; E: beam expander; P: the plate with a target on it; WP: wave plate; LP: linear polarizer.

where  $\theta_p$  represents the orientation of the polarizer. For the rotating wave plate, the Muller matrix of it should be

$$M_R(\Delta, \theta_R) = J(\theta_R) \begin{bmatrix} 1 & 0 & 0 & 0 \\ 0 & 1 & 0 & 0 \\ 0 & 0 & \cos \Delta & \sin \Delta \\ 0 & 0 & -\sin \Delta & \cos \Delta \end{bmatrix} J(-\theta_R) \quad (8)$$

where  $\theta_R$  and  $\Delta$  represent the orientation and phase shift of the wave plate, respectively.  $J(\theta_R)$  is a rotation matrix with the orientation of  $\theta_R$  given by

$$J(\theta_R) = \begin{bmatrix} 1 & 0 & 0 & 0 \\ 0 & \cos(2\theta_R) & -\sin(2\theta_R) & 0 \\ 0 & \sin(2\theta_R) & \cos(2\theta_R) & 0 \\ 0 & 0 & 0 & 1 \end{bmatrix}. \quad (9)$$

The phase shift of the wave plate  $\Delta$  depends on the wavelength  $\lambda$ . Therefore,  $M_R$  depends on the orientation of the wave plate and the wavelength of the light.

The Muller Matrix of PSA  $M$  could be defined as

$$M(\theta_p, \theta_R, \lambda) = M_P M_R. \quad (10)$$

The eigenstate of PSA at a certain wavelength  $\lambda$  should be the first row of matrix  $M$ , which is given by

$$\mathbf{T}(\lambda) = \begin{bmatrix} 1 \\ \frac{\cos(2\theta_p - 4\theta_R)(1 - \cos\Delta)}{2} + \frac{\cos 2\theta_p(1 + \cos\Delta)}{2} \\ \frac{\sin(2\theta_p - 4\theta_R)(\cos\Delta - 1)}{2} + \frac{\sin 2\theta_p(1 + \cos\Delta)}{2} \\ \sin \Delta \sin(2\theta_p - 2\theta_R) \end{bmatrix}. \quad (11)$$

It can be seen in (11) that the eigenstate of PSA  $\mathbf{T}$  depends on the orientation of the linear polarizer  $\theta_p$  and the orientation of the wave plate  $\theta_R$ . Therefore, the eigenstate of PSA  $\mathbf{T}$  can be adjusted by adjusting the orientations of the linear polarizer and the wave plate.

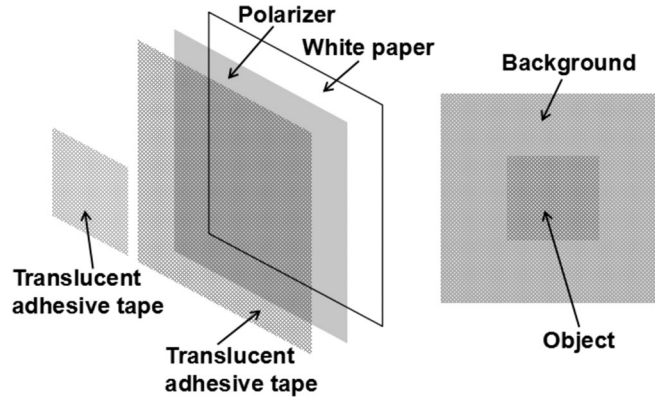


Fig. 3. Schematic of the scene.

Consequently, the measuring matrix  $W$ , which depends on the wavelength, can be expressed as

$$W(\lambda) = \frac{1}{2} \begin{bmatrix} \mathbf{T}_1(\lambda)^T \\ \mathbf{T}_2(\lambda)^T \\ \mathbf{T}_3(\lambda)^T \\ \mathbf{T}_4(\lambda)^T \end{bmatrix} \quad (12)$$

where  $\mathbf{T}_1$ ,  $\mathbf{T}_2$ ,  $\mathbf{T}_3$ , and  $\mathbf{T}_4$  stand for four different eigenstates of PSA.

The cross-talk effects in color CCD is caused by spectral overlapping of the Bayer filter in RGB channels, and in this case, the light at a certainly wavelength could generate the signals in multiple channels, as mentioned in Section 3. This could result in the distortion in the measurement of the light intensities at different wavelengths. Therefore, in order to properly measure the Stokes vector, one has to compensate the cross-talk effects mentioned above to get the light intensity correctly. This can be realized by taking into account the transfer efficiencies of R, G, and B channels for the wavelengths in the polarimetric system. It can be known from Fig. 1 that the transfer efficiencies for wavelengths of 450 nm, 532 nm and 633 nm in red channel are 0.0061, 0.0142, and 0.2678, respectively. The transfer efficiencies for these three wavelengths in green channel are 0.0497, 0.3010, and 0.0081, respectively, and those in blue channel are 0.2330, 0.0477, and 0, respectively. These transfer efficiencies for the wavelengths of 450 nm, 532 nm, and 633 nm in RGB channels can be written in a matrix form as

$$K = \begin{bmatrix} 0.0061 & 0.0142 & 0.2678 \\ 0.0497 & 0.3010 & 0.0081 \\ 0.2330 & 0.0477 & 0.0000 \end{bmatrix}. \quad (13)$$

We denote the measured intensity signals vectors in R, G, and B channels at four different states of PSA to be  $\mathbf{I}_R$ ,  $\mathbf{I}_G$ , and  $\mathbf{I}_B$ , respectively, and we denote the corresponding true light intensities at 450 nm, 532 nm, and 633 nm to be  $\mathbf{I}_{450}$ ,  $\mathbf{I}_{532}$ , and  $\mathbf{I}_{633}$ , respectively. According to (6), the relation between them can be expressed as

$$\begin{bmatrix} \mathbf{I}_{450} \\ \mathbf{I}_{532} \\ \mathbf{I}_{633} \end{bmatrix} = K^{-1} \begin{bmatrix} \mathbf{I}_R \\ \mathbf{I}_G \\ \mathbf{I}_B \end{bmatrix}. \quad (14)$$

By this way, we can compensate the distortion to obtain the true light intensities at different wavelengths under different polarization states of PSA.

In our experiment, the employed wave plate is the quarter wave plate at 633 nm, and the orientations of the linear polarizer and the wave plate is set to be  $(0^\circ, 0^\circ)$ ,  $(90^\circ, 0^\circ)$ ,  $(45^\circ, 45^\circ)$ , and  $(45^\circ, 0^\circ)$  to realize four eigenstates of PSA in order to make the measurement matrix  $W$  at 633 nm

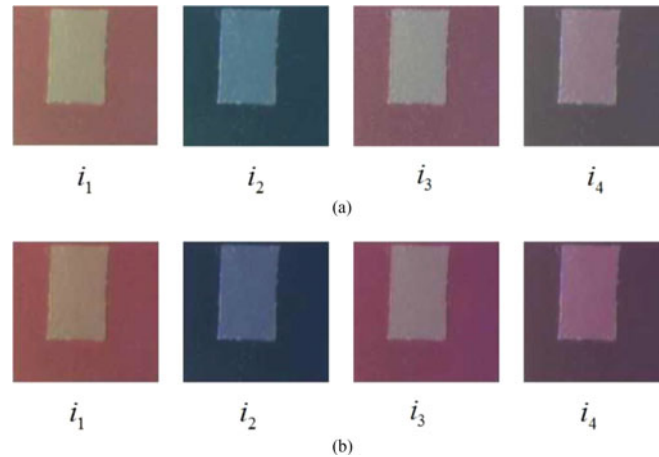


Fig. 4. (a) Initial RGB intensity images at four different eigenstates of PSA recorded by CCD. (b) Compensated intensity images at four different eigenstates of PSA.

to be

$$W_{633} = \frac{1}{2} \begin{bmatrix} 1 & 1 & 0 & 0 \\ 1 & -1 & 0 & 0 \\ 1 & 0 & 1 & 0 \\ 1 & 0 & 0 & 1 \end{bmatrix}. \quad (15)$$

The phase retardances of this wave plate at 450 nm and 532 nm are  $0.738 \pi$  and  $0.604 \pi$ , respectively. The orientations of the polarizer and the wave plate are same to those at 633 nm. Therefore, based on (11) and (12), the measurement matrix at 450 nm and 532 nm can be calculated to be

$$W_{450} = \frac{1}{2} \begin{bmatrix} 1 & 1 & 0 & 0 \\ 1 & -1 & 0 & 0 \\ 1 & 0 & 1 & 0 \\ 1 & 0 & -0.680 & 0.733 \end{bmatrix} \quad (16)$$

$$W_{532} = \frac{1}{2} \begin{bmatrix} 1 & 1 & 0 & 0 \\ 1 & -1 & 0 & 0 \\ 1 & 0 & 1 & 0 \\ 1 & 0 & -0.321 & 0.947 \end{bmatrix}.$$

The schematic of the scene to be measured is shown in Fig. 3. The background of the scene is a superposition of white paper, a sheet polarizer, and a translucent adhesive tape. The object consists of a piece of translucent adhesive tape placed on the background. Since adhesive tapes are birefringent materials whose retardances depend on the wavelength, the Stokes vectors of light scattered by the scene depends on the wavelength.

The initial intensity images at four different eigenstates of PSA, which are the RGB images recorded by the CCD, are shown in Fig. 4, and the corresponding compensated intensity images are shown in Fig. 4(b). It can be seen that Fig. 4(b) is slightly different from Fig. 4(a), which is attributed to the compensation of the cross-talk effect between RGB channels.

Based on the compensated intensity image in Fig. 4(b), the measured Stokes vector of the scattered light at 450 nm, 532 nm, and 633 nm is shown in Fig. 5 according to (4), (15), and (16). The color scale in Fig. 5 represents the values of the elements in the Stokes vector. It can be seen from Fig. 5 that the Stokes vectors of the scattered light at different wavelengths are considerably different from each other.

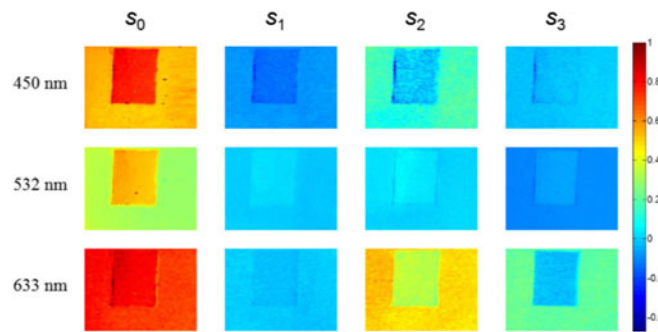


Fig. 5. Measured Stokes vectors of the scene at 450 nm, 532 nm, and 633 nm.

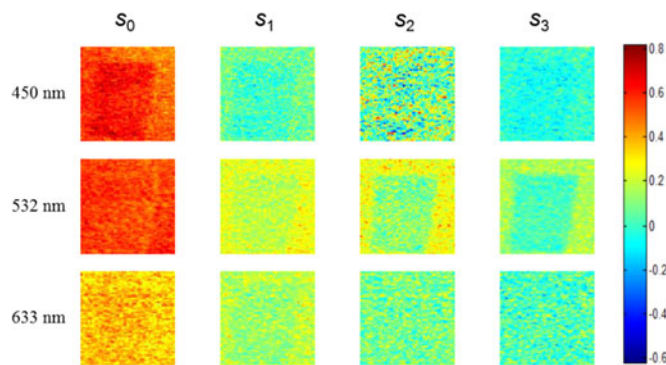


Fig. 6. Measured Stokes vectors of the scene at 450 nm, 532 nm, and 633 nm at low signal-to-noise ratio.

It needs to be clarified that the measurement of the Stokes vectors at three wavelengths shown in Fig. 5 is realized by capturing four RGB images at four different states of PSA by the color CCD. Compared with the previous Stokes imaging polarimetry at single wavelength [2], the method proposed in this paper can realize the measurement of the Stokes vectors at three wavelengths instead of at just one single wavelength, while keeping the times of modulating the state of PSA and the times of image capture unchanged.

The diversity of the Stokes vectors at different wavelengths, which is shown in Fig. 5, combines the polarization information and the spectral information, and it could be beneficial for various applications of polarimetry. In the following, we will present the experiment of target classification based on Stokes imaging polarimetry.

## 5. Target Classification by Multispectral Stokes Imaging Polarimetry

The method of measuring three-wavelength Stokes vectors could be widely employed in polarimetric imaging and polarimetric analyzing. One of the prominent applications is in classification or discrimination of the target. In order to compare the performances of classification at one single wavelength and at multiple wavelengths, we perform the corresponding experiment of Stokes imaging polarimetry.

The configuration of the target classification system is same to the imaging polarimetry system shown in Fig. 2. For the sake of simplicity, a scene with two different regions is investigated. The measured Stokes vectors of each pixel of the scene at three different wavelengths (450 nm, 532 nm and 633 nm) are shown in Fig. 6. It needs to be clarified that in this experiment, we fabricate the object whose Stokes vector is close to that of the background, especially at 633 nm. In addition,

we decrease the intensity of the light sources in the polarimetric system to decrease the signal to noise ratio. Therefore, the object is relatively hard to be discriminated in Fig. 6, compared with that in Fig. 5.

In the case of low light intensity, such as the case of Fig. 6, the noise should obey a Gaussian distribution [16], [17], and thus, it is assumed that the perturbation of the noise leads to Gaussian statistics for the measured data (the measured four elements in the Stokes vector). Therefore, we perform the polarimetric classification with Gaussian statistics.

Let us consider a target containing regions with different polarimetric properties with a number of  $N$ . It is assumed that the Stokes vector of each pixel in the scene can be obtained, and for a single pixel  $x$ , we have the Stokes vector in single wavelength as  $\mathbf{S}_x$ . The probability density function (PDF) associated with the region of class  $k$  in the scene will be [18]

$$P_k(\mathbf{S}_x) = \frac{1}{\sqrt{2\pi \det(\Gamma_k)}} \exp \left[ -\frac{1}{2} (\mathbf{S}_x - \bar{\mathbf{S}}_k)^T \Gamma_k^{-1} \right. \\ \left. \times (\mathbf{S}_x - \bar{\mathbf{S}}_k) \right], \quad k \in [1, N] \quad (17)$$

where  $\bar{\mathbf{S}}_k$  and  $\Gamma_k^{-1}$  are the mean and covariance of the Stokes vectors in region  $k$ , which are estimated based on the database pixels of region  $k$ . In fact, (17) is the extension of the PDF of Gaussian distribution from 1-D to multi-dimensional. The database pixels of region  $k$  could be defined as  $\Omega_k$ , and then, we have

$$\hat{\bar{\mathbf{S}}}_k = \frac{1}{P_{\Omega_k}} \sum_{x \in \Omega_k} \mathbf{S}_x \\ \hat{\Gamma}_k = \frac{1}{P_{\Omega_k}} \sum_{x \in \Omega_k} (\mathbf{S}_x - \bar{\mathbf{S}}_k)(\mathbf{S}_x - \bar{\mathbf{S}}_k)^T \quad (18)$$

where  $P_{\Omega_k}$  is the number of pixels in  $\Omega_k$ . If a pixel  $x$  is recognized as in region  $k$  of the scene, then  $k$  should maximize the likelihood function given by (17), which is expressed as [19]

$$\hat{k} = \arg \max_{k \in [1, N]} \{ \log [P_k(\mathbf{S}_x)] \}. \quad (19)$$

In this way, we can perform target classification. Actually, the basic idea of the classification algorithm above is to find the region of class  $k$  with the maximum probability density for the pixel  $x$ , which is identified to be the class that the pixel  $x$  belongs to. In practice, the probability densities of all the region of classes for pixel  $x$  are calculated, and consequently, the region of class with the maximum probability density can be identified.

It needs to be clarified that the classifier in (19) is based on the Stokes vector at one single wavelength with the dimensions of four, and it can be directly extended to higher dimensions by basing on the Stokes vectors at multiple wavelengths. In our case, we can combine the Stokes vectors at three wavelengths into a 12-D vector. Adapting this 12-D vector to (17) and (19), one can realize the classification based on the Stokes vectors at three wavelengths.

We perform the experiment of classification based on the Stokes vectors at single wavelength of 450 nm, 532 nm, and 633 nm, respectively. In addition, we also perform the classification based on the Stokes vectors at three wavelengths for the purpose of comparison. The results of classification are shown in Fig. 7, in which the blue and red pixels in Fig. 7 refer to the pixels classified to be the background and the target, respectively.

It can be seen in Fig. 7(a) to (c) that due to the low signal to noise ratio as well as the similarity between the Stokes vectors of the object and background, the target classification at single wavelength induce misclassification at many pixels, especially in Fig. 7(c). In fact, in the case of one single wavelengths, the Stokes vector of the target could be too close to that of the background, which could induce the failure of target classification (or discrimination), as the case for the wavelength of 633 nm shown in Fig. 7(c). However, for the classification based on the Stokes vectors

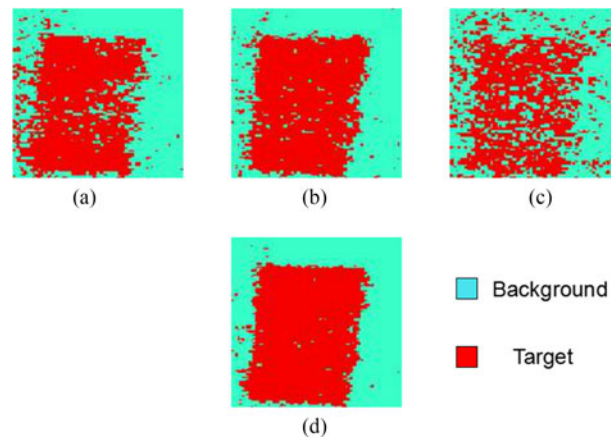


Fig. 7. Result of classification at different wavelengths (a) at 450 nm, (b) at 532 nm, (c) at 633 nm, and (d) at three wavelengths.

at three wavelengths, due to eight additional dimensions compared with that for single-wavelength, we could significantly improve the accuracy of classification. As Fig. 7(d) shows, the classification errors in the scene is significantly decreased, and the target and background can be identified with a good performance, which is even better than that at 532 nm [ see Fig. 7(b)], which performs best among Fig. 7(a) to (c). Therefore, the method of multispectral Stokes imaging polarimetry based on color CCD can increase the classification performance, due to the ability of simultaneously obtaining the Stokes vectors at three wavelengths. In addition, it can considerably decrease the possibility of the failure of target discrimination, which could happen for one single wavelength.

It needs to be clarified that the experiment above is based on the Stokes polarimetry, while the performance of the target discrimination or classification can be improved by Mueller polarimetry, which can realize the proper choice of input Stokes vector to benefit the target discrimination or classification.

## 6. Conclusion

In conclusion, the method of multispectral imaging polarimetry based on color CCD is proposed, which can obtain the Stokes vectors of the scene at three different wavelengths simultaneously. Compared with the typical imaging polarimetry for one wavelength, this method can provide more spectral polarization information without significantly increasing the complexity of the system and the procedure for the polarimetry. In addition, it is shown by the experimental result that, the performance of target classification or detection can be improved by employing this method, thanks to the diversity of the polarization information at different wavelengths. Actually, the method proposed in this paper can significantly increase the amount of obtained polarimetric information and can effectively overcome the failure of polarimetric target detection at single wavelength.

The method of multispectral imaging polarimetry based on color CCD proposed in this paper goes beyond the particular case of Stokes imaging polarimetry, and it can be extended to other types of polarimetry, such as Mueller imaging polarimetry [20], [21] and orthogonal state contrast (OSC) imaging polarimetry [22].

## References

- [1] G. Anna, F. Goudail, and D. Dolfi, "Polarimetric target detection in the presence of spatially fluctuating Mueller matrices," *Opt. Lett.*, vol. 36, no. 23, pp. 4590–4592, 2011.
- [2] B. Huang, T. Liu, J. Han, and H. Hu, "Polarimetric target detection under uneven illumination," *Opt. Exp.*, vol. 23, no. 18, pp. 23603–23612, 2015.

- [3] M. Boffety, H. Hu, and F. Goudail, "Contrast optimization in broadband passive polarimetric imaging," *Opt. Lett.*, vol. 39, no. 23, pp. 6759–6762, 2014.
- [4] F. Goudail and A. Bénére, "Optimization of the contrast in polarimetric scalar images," *Appl. Opt.*, vol. 34, no. 9, pp. 1471–1473, 2009.
- [5] S. Tyo, D. L. Goldstein, D. B. Chenault, and J. A. Shaw, "Review of passive imaging polarimetry for remote sensing applications," *Appl. Opt.*, vol. 45, no. 22, pp. 5453–5469, 2006.
- [6] A. Pierangelo *et al.*, "Ex-vivo characterization of human colon cancer by Mueller polarimetric imaging," *Opt. Exp.*, vol. 19, no. 2, pp. 1582–1593, 2011.
- [7] M. Alouini, F. Goudail, P. Réfrégier, A. Grisard, E. Lallier, and D. Dolfi, "Multispectral polarimetric imaging with coherent illumination: Towards higher image contrast," *Proc. SPIE*, vol. 5432, pp. 133–144, 2004.
- [8] Y. Shkuratov *et al.*, "Multispectral polarimetry as a tool to investigate texture and chemistry of lunar regolith particles," *Icarus*, vol. 187, no. 2, pp. 406–416, 2007.
- [9] A. Pierangelo *et al.*, "Multispectral Mueller polarimetric imaging detecting residual cancer and cancer regression after neoadjuvant treatment for colorectal carcinomas," *J. Biomed. Opt.*, vol. 18, no. 4, 2013, Art. no. 046014.
- [10] S. G. Demos, H. B. Radousky, and R. R. Alfano, "Deep subsurface imaging in tissues using spectral and polarization filtering," *Opt. Exp.*, vol. 7, no. 1, pp. 23–28, 2000.
- [11] G. C. Giakos, "Multifusion multispectral lightwave polarimetric detection principles and systems," *IEEE Trans. Instrum. Meas.*, vol. 55, no. 6, pp. 1904–1912, Jan. 2006.
- [12] N. Gupta, L. J. Denes, M. Gottlieb, D. R. Suhre, B. Kaminsky, and P. Metes, "Object detection with a field-portable spectropolarimetric imager," *Appl. Opt.*, vol. 40, no. 36, pp. 6626–6632, 2001.
- [13] N. Gupta, "Acousto-optic-tunable-filter-based spectropolarimetric imagers for medical diagnostic applications-instrument design point of view," *J. Biomed. Opt.*, vol. 10, no. 5, 2005, Art. no. 051802.
- [14] S. Knitter, T. Hellwig, M. Kues, and C. Fallnich, "Spectrally resolving single-shot polarimeter," *Opt. Lett.*, vol. 36, no. 16, pp. 3048–3050, 2011.
- [15] A. Beniere, M. Alouini, F. Goudail, A. Grisard, J. Bourderionnet, D. Dolfi, I. Baarstad, T. Loke, P. Kaspersen, X. Normandin, and G. Bergine, "Snapshot active polarimetric and multispectral laboratory demonstrator," *Proc. SPIE*, vol. 7323, 2009, Art. no. 732710.
- [16] J. S. Tyo, "Design of optimal polarimeters: Maximization of the signal-to-noise ratio and minimization of systematic error," *Appl. Opt.*, vol. 41, no. 4, pp. 619–630, 2002.
- [17] G. Anna, F. Goudail, P. Chavel, and D. Dolfi, "On the influence of noise statistics on polarimetric contrast optimization," *Appl. Opt.*, vol. 51, no. 8, pp. 1178–1187, 2012.
- [18] G. Anna, F. Goudail, and D. Dolfi, "Optimal discrimination of multiple regions with an active polarimetric imager," *Opt. Exp.*, vol. 19, no. 25, pp. 25367–25378, 2011.
- [19] H. Hu, G. Anna, and F. Goudail, "On the performance of the physicality-constrained maximum-likelihood estimation of Stokes vector," *Appl. Opt.*, vol. 52, no. 27, pp. 6636–6644, 2013.
- [20] B. L. Boulestelx, A. D. Martino, B. Drévilon, and L. Schwartz, "Mueller polarimetric imaging system with liquid crystals," *Appl. Opt.*, vol. 43, no. 14, pp. 2824–2832, 2004.
- [21] J. L. Pezzaniti and R. A. Chipman, "Muller matrix imaging polarimetry," *Opt. Eng.*, vol. 34, no. 6, pp. 1558–1568, 1995.
- [22] G. Anna, F. Goudail, and D. Dolfi, "General state contrast imaging: An optimized polarimetric imaging modality insensitive to spatial intensity fluctuations," *J. Opt. Soc. Amer. A*, vol. 29, no. 6, pp. 892–900, 2012.